

A Complex Study of the Peculiarities of Blood Serum Absorption of Rats with Experimental Liver Cancer¹

M. M. Nazarov^a, O. P. Cherkasova^{b, c, d, *}, E. N. Lazareva^{c, e}, A. B. Bucharskaya^f,
N. A. Navolokin^g, V. V. Tuchin^{c, e, g}, and A. P. Shkurinov^{h, i}

^a National Research Centre Kurchatov Institute, Moscow, 123182 Russia

^b Institute of Laser Physics, Siberian Branch, Russian Academy of Sciences, Novosibirsk, 630090 Russia

^c Tomsk State University, Tomsk, 634050 Russia

^d Novosibirsk State Technical University, Novosibirsk, 630073 Russia

^e Saratov State University, Saratov, 410012 Russia

^f Saratov State Medical University, Saratov, 410012 Russia

^g Institute of Precision Mechanics and Control, Russian Academy of Sciences, Saratov, 410028 Russia

^h Moscow State University, Moscow, 119991 Russia

ⁱ Institute for Problems of Laser and Information Technologies of the Russian Academy of Sciences,
Branch of Federal Scientific Research Center Crystallography and Photonics, Shatura, 140700 Russia

*e-mail: o.p.cherkasova@gmail.com

Received December 17, 2018; revised February 13, 2019; accepted February 26, 2019

Abstract—Terahertz time-domain spectroscopy (THz-TDS) in the 0.05–1.0 THz frequency range was used to study the blood serum of rats in the dynamics of experimental liver cancer. It was shown that the THz transmission spectra of samples from healthy animals and 14 and 28 days after tumor cells implantation are similar in shape, but differ in amplitude. There is a change in the biochemical composition of the blood, including a decrease in the protein content, by the 28th day of the experiment. The observed changes in the THz response are explained by a decrease in the number of protein molecules and bound water and correlate with changes in the refractive index in the visible and near-IR ranges from 480 to 1550 nm, measured using a multiwave refractometer.

DOI: 10.1134/S0030400X19060183

INTRODUCTION

The high water content in biological liquids and in the vast majority of biological tissues determines the nature of their dielectric response in the terahertz (THz) frequency range of the electromagnetic spectrum [1]. The measured characteristic in THz spectroscopy is the state of the water itself prevailing in biological samples, which, as is well known, can be in a free and bound state [2]. The THz frequency range reflects the changes in the proportions of free and bound water and differences in relaxation times for each of these states. Sensitivity to the presence of free water has a range from 0.01 to 1 THz, since the characteristic frequency of the peak absorption of free water corresponds to 20 GHz, and its spectral width

extends by 2–3 octaves in both directions [3]. Therefore, to increase the sensitivity of the THz spectroscopy, it is necessary to expand the dynamic range of the THz spectrometer towards low frequencies.

The frequency dependence of the complex dielectric THz permeability of water and biological tissues is described by relaxation models, for example, the double Debye model with very close parameters [1, 4–6]. The relaxation dielectric response of tissues and solutions is characterized by the absence of clearly defined spectral features in the THz frequency range of 0.1–3 THz. At the same time, the sensitivity of radiation to water content makes THz spectroscopy and visualization attractive medical diagnostic tools using the water content in tissues and its state as informative features to differentiate [7–9].

Blood is a complex system consisting of plasma and cellular elements suspended in it. Blood plasma is about 90% of water and about 6.6–8.5% proteins and other organic and mineral compounds, which are intermediate or end products of metabolism carried by blood [10]. Various components of blood have a sig-

¹ The 22nd Annual Conference Saratov Fall Meeting 2018 (SFM'18): VI International Symposium "Optics and Biophotonics" and XXII International School for Junior Scientists and Students on Optics, Laser Physics, and Biophotonics, September 24–29, 2018, Saratov, Russia. <https://www.sgu.ru/structure/fiz/saratov-fall-meeting/previousconferences/saratov-fall-meeting-2018>

nificant impact on its optical properties, and their contribution may change with the development of pathological conditions. A number of authors believe that the blood levels of triglycerides [11] and creatinine [12] have a significant effect on the absorption coefficient and the refractive index in the range of 0.2–1.0 THz. The number of erythrocytes in the blood negatively correlates with the absorption coefficient in the THz-spectral region [6, 11, 13]. Blood clot formation during blood coagulation has a significant effect on the absorption coefficient at 200–270 GHz [14]. The effect of the glucose concentration in the blood on its optical properties in the THz frequency range is most reliably studied [15, 16]. The analysis of the blood of 70 patients has demonstrated that the absorption coefficients in the THz spectral region and the levels of glucose in the blood had a linear relationship [16].

We have previously shown that the absorption coefficient and the refractive index of blood plasma of rats with experimental diabetes, measured in the frequency range 0.2–2.0 THz, are significantly lower, and the phase of the reflection coefficient is higher than these parameters in healthy animals [17]. Rats with diabetes have a blood glucose content of 3.7 times higher than healthy rats. Assuming that the observed spectral changes are due to changes in the state of water in the blood plasma, it was shown that the ratio $\Delta\epsilon_1/\tau_1$ decreases by a factor of 1.2 in the main relaxation term in the Debye model (see expression (5) below) in rat blood plasma with increasing glucose concentrations up to 24 mM [17].

It was also determined that the absorption of plasma from rats with severe experimental diabetes is more than two times less than this value for rats with uncomplicated diabetes [18]. The content of glucose and protein in the blood plasma of rats, i.e., substances that may have a significant effect on the state of water in the THz range [19–21] did not differ statistically significantly. This suggests that some components that are contained in the blood plasma during complicated diabetes may contribute to the total absorption. One such component may be glycation products. A significant increase in the fluorescence of blood plasma of diabetic rats was shown when excited at a wavelength of 320 nm, indicating an increase in the number of final glycation products [22].

A decrease in the absorption coefficient of blood plasma of mice with transplanted Ehrlich carcinoma in the THz-region of the spectrum was demonstrated [23]. The authors suggested that this difference may be caused by changes in the composition of blood plasma during the carcinoma development.

Thus, analysis of published data shows that a change in the blood composition at pathologies can have a significant impact on the change in the blood optical properties in the THz frequency range. This can be used to create new methods for the rapid diag-

nosis of various diseases. Identification of cancer pathology at early stages and the search for objective criteria for predicting the dynamics of the disease development and treatment are important. Cholangiocarcinoma (alveolar liver cancer) is a malignant tumor that is formed from mutated epithelial cells of the bile ducts. The incidence of this type of cancer has increased significantly in recent years [24]. It is characterized by a long period of the asymptomatic course and is found, as a rule, in the latter stages of the course of the disease, when the prognosis for cure is unsatisfactory.

This paper is devoted to studying the optical characteristics of rat blood serum in the THz frequency range in the dynamics of cholangiocarcinoma, identifying differences between samples from healthy and experimental animals, comparing data with the biochemical composition of blood and the results of refractometry in the visible/IR wavelength ranges.

MATERIALS AND METHODS

Methods of Measurement and Processing the Spectral Data

We used a THz-TDS spectrometer, the detailed description of which was published earlier [17, 19, 21]. A specific feature of this laboratory spectrometer is its relatively high average power of THz radiation, which is 10 μW (from a photoconductive multidipole antenna and 1 W of laser femtosecond radiation) [25], which allows a 0.5-mm-thick water sample to be transmitted up to 1 THz (Fig. 1). Since we investigated substances in the form of solutions in water, which has a strong absorption and dispersion due to the relaxation process in the region of 10–100 GHz [1, 3], the dynamic range of the THz spectrometer was optimized at low frequencies till 0.05 THz. In Fig. 1, the extended range of the spectrometer is highlighted in dark gray compared with the usual for TDS THz spectrometers. Fig. 1a shows the spectrum of the imaginary part of dielectric constant ϵ for the three components of the aqueous solution (for bound water according to dielectric spectroscopy [26]), and Fig. 1b shows the dynamic range of the used low-frequency spectrometer configuration.

For a sufficient signal-to-noise ratio, when measuring at extremely low frequencies (of the order of 0.05 THz), a long-time sample was used, namely, from -20 to 40 ps relative to the center of the THz pulse. The signal profiles ($A(t)$ in Fig. 2) were recorded with a time step of 0.05 ps. To increase the reliability of measurements, each serum sample was analyzed in triplicates, then these three independent measurements were averaged. The time dependence of the electric field of the THz pulse $A(t)$ was transformed by the Fourier transform into its spectral domain $E(f)$ (Fig. 1b), where t is time and f is frequency. Experimental samples were placed in a liquid cell (Bruker,

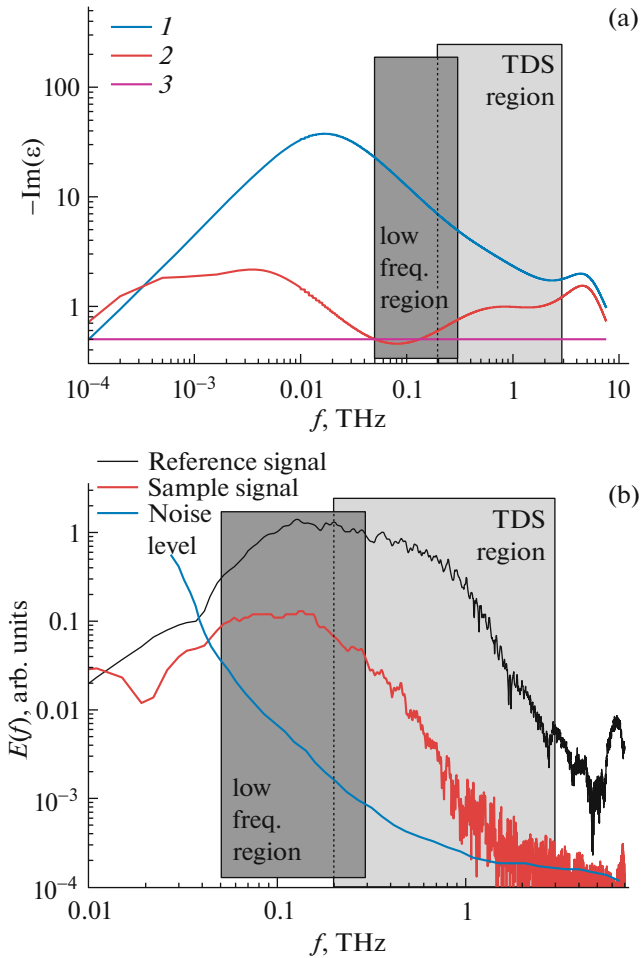


Fig. 1. (a) The spectrum of the imaginary part of the dielectric constant ϵ for the three components of the aqueous solution: (1) free water spectrum (blue line); (2) bound water spectrum [26] (red line); (3) solute spectrum (pink line); (b) the dynamic range of the used THz spectrometer: the spectrum of the incident radiation is the black line; the spectrum of the $E(f)$ signal passed through 500 μm of water is the red line; noise level is the blue line. The low-frequency part of the THz spectrum is highlighted in dark gray; the traditional range for THz-TDS is highlighted in gray.

United States) with two identical polystyrene windows. Refractive index of windows $n_c = 1.5$ and is constant in the used frequency range. The thickness of the liquid layer in our experiment was $500 \pm 5 \mu\text{m}$. The cell was installed in a collimated THz beam. Note that such a relatively large thickness of the solution layer is necessary to ensure the accuracy of measurements in the used frequency range. The thickness of the layer was set by a Teflon spacer between the windows, the same for all measurements. All measurements were carried out at room temperature of $21 \pm 1^\circ\text{C}$. The transmission of the blood serum $T_w(f)$ was analyzed after normalization to the signal passing through the

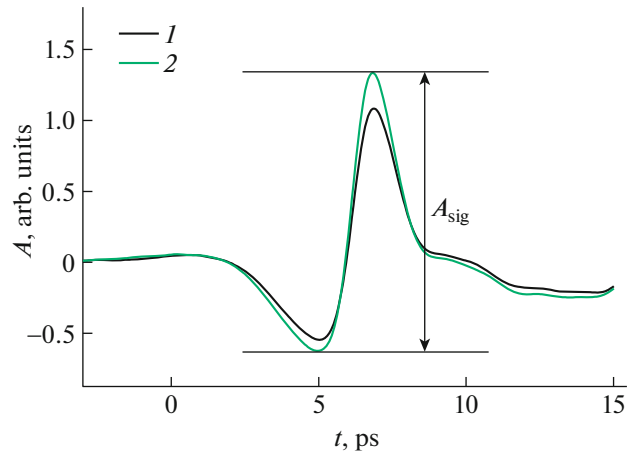


Fig. 2. Time profile $A(t)$ and peak signal amplitude A_{sig} : 1, signal passed through 500 μm of water (black line), 2, signal passed through 500 μm of blood serum (green line). The zero-time point corresponds to the maximum pulse transmitted through the layer of air.

distilled water $E_{\text{water}}(f)$ in the same cell, measured regularly in turn with the serum:

$$T_w(f) = \frac{E_{\text{sample}}(f)}{E_{\text{water}}(f)}. \quad (1)$$

Such approach to normalization allows to measure small spectra changes more accurately. We used similar method earlier in the study of the blood plasma of diabetic rats [17, 18].

The full amplitude of the A_{sig} THz pulse time profile was determined for an integral assessment of the difference in the THz response of blood serum from the response of water (Fig. 2). This value was also analyzed after normalization to the reference signal passing through the water:

$$T_p = \frac{(A_{\text{max}}^{\text{sig}} - A_{\text{min}}^{\text{sig}})}{(A_{\text{max}}^{\text{w}} - A_{\text{min}}^{\text{w}})}, \quad (2)$$

where “sig” is a sample, “w” is a reference signal passing through the water, and $A_{\text{sig}} = A_{\text{max}}^{\text{sig}} - A_{\text{min}}^{\text{sig}}$ is shown in Fig. 2.

Considering that the spectrum of the transmitted signal is located (at a level of 0.5) between 0.1 and 0.3 THz (Fig. 1b), the value of T_p is equal to relative transmittance T_w averaged over this frequency range. This approximately corresponds to T_w (0.2 THz) and values of 1.13–1.22 for the three groups of samples studied (Figs. 3, 4).

To recalculate the transmission spectrum into the absorption coefficient and refractive index spectra (with normalization to the incident signal $E_0(f)$), the Fresnel equations and methods described in [17, 19, 21, 27, 28], as well as formulas (8) and (9) (see below) in the case of normalization to water were used.

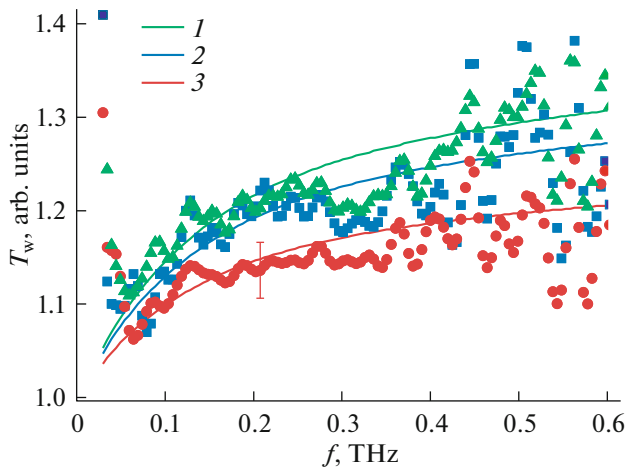


Fig. 3. Transmission spectra of blood serum normalized to the transmission spectrum of the cuvette with water, T_w . The dots show the mean transmission amplitude for each group: group 1, green triangles, group 2, blue squares, group 3, red circles. Solid colored lines are reduced amplitude $\Delta\epsilon_1$ model spectra: (1) for group 1, (2) for group 2, (3) for group 3.

There is an unambiguous connection between the measured complex transmittance $T_0(f) = E(f)/E_0(f)$ and the dispersion of the dielectric constant of the substance under study [19], as well as the dispersion of its absorption coefficient and refractive index. In a simplified form, the frequency dependences of absorption coefficient $\alpha(f)$ and the refractive index $n(f)$ can be represented as follows:

$$\alpha(f) = -\frac{\ln\left[|T_0(f)|\frac{(n_c + n(f))^2}{4n_c n(f)}\right]}{d}, \quad (3)$$

$$n(f) = -\arg[T_0(f)]\frac{c}{2\pi f d} + 1,$$

where d is a sample thickness and c is the speed of light. At the same time, $\epsilon(f) = n^*(f)^2$ is the relationship of the complex refractive index of the sample with the dielectric constant, where

$$n^*(f) = n(f) + i\frac{\alpha(f)c}{2\pi f}. \quad (4)$$

Factor $\frac{(n_c + n(f))^2}{4n_c n(f)}$ in (3) is needed at low frequencies to account for losses due to reflection from the boundaries of water. Note that, in this paper, we use the absorption coefficient for the amplitude of the field, and not for the power, which is twice as large and generally accepted. Instrumental errors associated with the accuracy of determining the thickness of the solution in the cell and the drift of the baseline ultimately lead to a total error of 5%. The results for $\epsilon(f)$, recal-

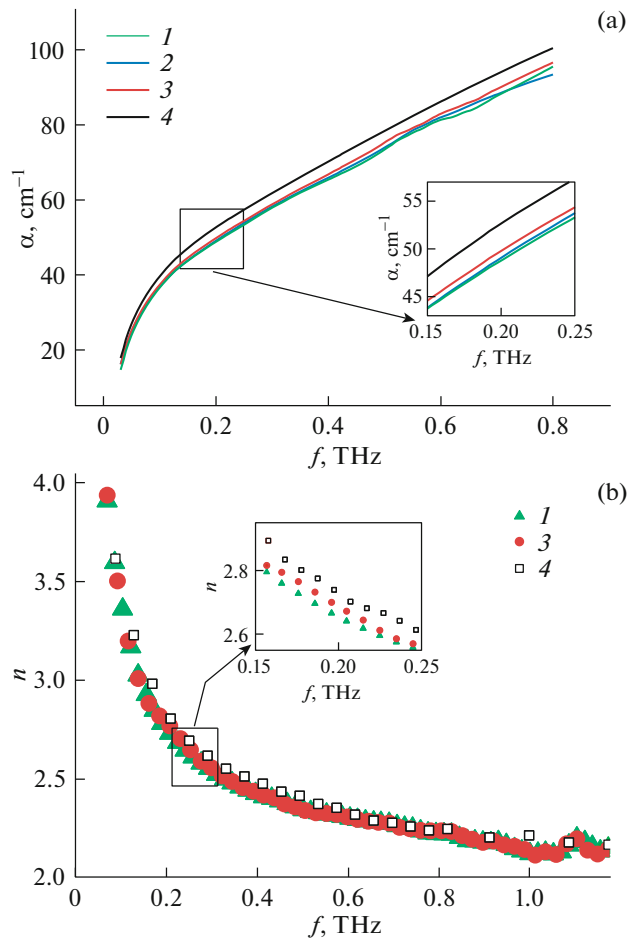


Fig. 4. (a) Absorption coefficient spectra for water and serum samples: (1) is group 1, green line; (2) is group 2, blue line; (3) is group 3, red line; (4) is water, black line; (b) refractive index spectra for serum samples: (1) is group 1 (triangles), (3) is group 3 (circles), (4) is water (squares).

culated from the transmission data, differs even with account of this value. The error/repeatability deteriorates up to 20% at the edges of the frequency spectrum (0.05–0.07 and 0.8–1.0 THz) due to the small value of the signal. The approximate formula (3) introduces an error of less than 1% in calculations of the absorption for frequencies greater than 0.05 THz and a layer of an aqueous solution of at least 0.5 mm.

Animal Characteristics

An experimental study was carried out on white outbred adult male rats according to the procedure described in [29]. Experiments on animals were performed in accordance with international ethical standards [30]. In this study, the development of alveolar liver cancer (cholangiocarcinoma, PC1) was initiated by injecting 0.5 mL of 25% tumor suspension in Hank’s balanced salt solution subcutaneously in the area of the scapula. Animals were analyzed on the 14th

Table 1. Protein and glucose content in the blood plasma of experimental animals and tumor mass

Group ($n = 8$)	Rat mass, g	Tumor mass, g	Total protein, g/L	Albumin, g/L	Glucose, M/L
Group 1 (healthy animals)	400–500	–	83 [67, 86.3]	37 [35.5, 39.3]	5.2 [4.9, 5.7]
Group 2 (14 days after tumor implantation)	150–200	0.98	73 [69.5, 77.3]	39 [36.5, 40.8]	7.8* [6.7, 8.9]
Group 3 (28 days after tumor implantation)	150–200	26.27	57** [55, 64]	21** [19, 23]	5.4 [5, 5.7]

Reliability of differences: * $p \leq 0.05$ compared with group 1; ** $p \leq 0.01$ compared with group 1.

and 28th day after tumor implantation. Body weight and tumor size were measured. The true body weight of the experimental animals was calculated by subtracting the tumor mass from the total body mass. Blood sampling was carried out in special tubes with coagulant. The serum was separated after 10 min of centrifugation, and then was used for biochemical analysis and spectral measurements.

Biochemical studies were conducted on the Clima MC-15 semiautomatic analyzer (RAL, Spain) using reagent kits for determining total protein, albumin, and glucose (Diacon-DS, Russia).

Animals were divided into three groups with eight individuals in each: group 1, control healthy animals; group 2, animals 14 days after tumor implantation; and group 3, animals 28 days after tumor implantation. The main characteristics of the animals are shown in Table 1. The number of animals in each group during spectroscopic studies was as follows: group 1—8, group 2—4, group 3—6 individuals.

Refractometry

The same serum samples were used to measure the refractive index in the visible and near-IR ranges on an Abbe DR-M2/1550 multiwave refractometer (Atago, Japan) with temperature stabilization. For wavelength selection, the following narrowband interference filters were used: 480, 486, 546, 589, 644, 656, 680, 800, 930, 1100, and 1550 nm. The measurement error introduced by the device was ± 0.0002 .

Statistical Data Analysis

To process the data obtained in the course of research, the applied statistical software package SPSS-13.0 was used. The normality of the distribution of values in the sample was checked using the Kolmogorov–Smirnov test. We calculated the arithmetic mean (M), the standard deviation, in the case of differences from the normal distribution the median and quartiles were used. The indicator of the reliability of differences (P) was determined using Student's criteria (t) and Mann–Whitney if the distribution differed from the normal one. To formalize the correspondence of optical parameters in the visible/IR and THz regions of the spectrum, the Pearson correlation coef-

ficient was calculated, which allows one to estimate linear relations between two variables.

RESULTS AND DISCUSSION

In the dynamics of tumor development, a statistically significant decrease in the concentration of both total protein and serum albumin is observed (Table 1). The albumin content in the blood serum of rats of group 3 (28 days after tumor implantation) is almost two times less than in the blood of healthy rats and rats of group 2 (14 days after tumor implantation). In the THz transmission spectra, differences were found between the samples for all studied animal groups (Fig. 3). The analysis of the observed differences was performed by comparing the experimental spectra obtained with the recalculation of the same dependencies from the model dielectric function of water $\epsilon(f)$:

$$\epsilon(f, C) = \epsilon_{\infty} + \frac{\Delta\epsilon_1(C)}{1 + i2\pi f\tau_1} + \frac{\Delta\epsilon_2}{1 + i2\pi f\tau_2} + \frac{A_1}{\omega_{01}^2 - (2\pi f)^2 + i\gamma_{01}2\pi f} + \dots \quad (5)$$

The values for the parameters in (5) were refined for distilled water in the corresponding frequency range for each of the considered processes [19]. So, for the most essential process of slow Debye relaxation ($\Delta\epsilon_1$, τ_1), which dominates in the frequency range of 1–100 GHz (centered at 20 GHz), the values are chosen from the data of dielectric spectroscopy. The parameters of the fast Debye process ($\Delta\epsilon_2$, τ_2) are consistent with the data of TDS THz spectroscopy. For the high-frequency Lorentz term (A_1 , ω_{01} , γ_{01}), data is selected from the results of IR Fourier transform spectroscopy, since the oscillatory processes begin to manifest from 4 THz and above. Finally, the following parameters are obtained: $\Delta\epsilon_1 = 72 \pm 1$, $\tau_1 = 9.96 \pm 0.5$ ps, $\Delta\epsilon_2 = 1.66 \pm 0.03$, $\tau_2 = 0.24 \pm 0.01$ ps, $A_1 = 31$ (THz 2π)², $\omega_{01}/2\pi = 5.3$ THz, and $\gamma_{01}/2\pi = 7$ THz. The sum of the amplitudes of all the considered processes determines the remainder of the static susceptibility in the form $\epsilon_{\infty} = 2.6 \pm 0.2$. The given set of values is optimal for the frequency range 0.05–2.5 THz at a temperature 21–24°C. The spectrum calculated using these values from (5) is shown in Fig. 1a by line I .

Previously, we have shown the validity of the simple model $\epsilon(f)$ for standard solutions of albumin and glucose in water [16, 19–21]. The essence of model (5) is that in the THz frequency range any aqueous solution of biomolecules can be described with enough accuracy by the dielectric constant of the water spectrum with a single change in the amplitude of the first, slow Debye relaxation. The concentration of the solute should be involved, as in the THz range any aqueous solution of biomolecules, including blood serum, can be described with sufficient accuracy mainly by reducing the amplitude of the “slow” component of Debye relaxation $\Delta\epsilon_1$ with an increase in the concentration of the dissolved substance C . In particular,

$$\Delta\epsilon_1(C) = \Delta\epsilon_1(1 - CK). \quad (6)$$

Empirical coefficient K at $\Delta\epsilon_1$ is uniquely related to concentration of the solute C and thus affects the spectrum of the dielectric function of the final solution. We previously showed that for albumin solution in water $K = 8 \times 10^{-4}$ mL/mg should be used [19]. For the other components of the serum, the K value is of the same order of magnitude [1]. Simplified formulas (5) and (6) are applicable in the frequency range 0.01–2.5 THz since the bound water formed has relaxation time τ_1 outside the specified range (Fig. 1a) and turns off some of the water molecules from the slow relaxation process with dominant absorption.

To obtain a model spectrum of the dielectric constant of serum of group 1 (control animals, protein concentration is 83 g/L) $\Delta\epsilon_1$ should be multiplied to 0.9; for group 2 (protein concentration is 73 g/L), to 0.91; and for group 3, having low protein level (57 g/L), to 0.93 (Fig. 3). The physical meaning of the approximated in the model parameter $(1 - CK) = \Delta\epsilon_{1, \text{water}}/\Delta\epsilon_{1, \text{solution}}$ is the volume fraction of free water in the solution. The remaining volume is occupied by bound water and solute molecules; both components have negligible absorption compared with free water in the studied range of 0.05–1.0 THz (Fig. 1a) [1].

To determine the value $(1 - CK)$, the measured spectra of blood serum samples from different groups of animals in the form of T_w (1) were compared with the model transmission, converted from dielectric constant $\epsilon(f)$ (5) and (6) as

$$T_w(f) = \exp\left\{-\frac{i[\epsilon_s(f)^{0.5} - \epsilon_w(f)^{0.5}]d2\pi f}{c}\right\}. \quad (7)$$

Note that approximate formula (7) does not consider reflections at the boundaries of the aqueous solution. This underestimates the value of T_w compared to (1) by no more than 0.02 for frequencies below 0.1 THz with the parameters used in the work. The largest differences in transmission spectra were observed for samples of group 3 relative to group 1: transmission for serum samples of animals of group 3, which are characterized by a statistically significantly

lower protein content in the blood, was less than for serum samples of healthy rats (Fig. 3). Each sample was independently measured three times. It is seen that the most reliable range of spectral values lies in the range from 0.07 to 0.5 THz.

From the transmission spectra T_w (1) normalized to water, one can calculate the change in the absorption coefficients and refractive indices:

$$\Delta\alpha = -\frac{\ln(|T_w|)}{d}, \quad \Delta n = -\frac{\arg(T_w)c}{2\pi fd}. \quad (8)$$

Then, if the frequency dependence of the reference spectrum of water (5) is well known, it is possible to restore the absorption and refraction spectra of the studied solutions without additional simplifications, errors, and noises (Fig. 4):

$$\alpha_{\text{solution}}(f) = \text{Im}[\epsilon(f)^{0.5}] \frac{2\pi f}{c} + \Delta\alpha(f), \quad (9)$$

$$n_{\text{solution}}(f) = \text{Re}[\epsilon(f)^{0.5}] + \Delta n(f).$$

The largest differences are observed in the spectrum of the absorption index in comparison with the spectrum of the refractive index (Fig. 4). The shape of the spectra of water and serum coincides, but there is a difference in amplitude. To identify the weak differences between the studied samples we used the method of normalization to the signal passing through the water, as described above. We note that if reflections (which are canceled out in the first approximation) are not considered in formulas (1) and (7)–(9), the error in determining α and n is less than 0.5 cm^{-1} and 0.02, respectively, which is negligible.

If the dielectric function of the studied samples is known, it is possible to calculate the amplitude of the reflection coefficient [17] and in the future apply THz spectroscopy for contactless diagnostics, as we tested earlier for noninvasive determination of blood glucose [30]. We recorded changes in the parameters of the reflection signal from the skin depending on the change in the glucose content in human blood [31]. For realistic concentrations of blood components, the differences in refractive indices are small for the current accuracy of the experiment. We recalculate the amplitude of reflection from the model permeability as

$$R = \left| \frac{(1 - \epsilon^{0.5})}{(1 + \epsilon^{0.5})} \right|. \quad (10)$$

The difference in the amplitude of the reflected signals for samples from groups 1 and 3, recalculated as $R(\epsilon_{\text{Group3}}) - R(\epsilon_{\text{Group1}})$, is estimated at 0.6% (Fig. 5). In this case, the maximum sensitivity (within the framework of models (5) and (6)) is expected to be in the region of 0.1–0.3 THz. With an increase in the dynamic range of the THz devices by two orders of magnitude, it will be possible to record in the future such a small difference in the reflection and use these

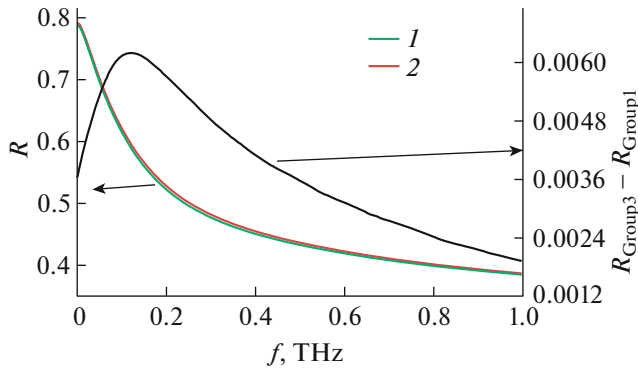


Fig. 5. The calculated reflection spectra for serum samples of groups 1 (green line) and 3 (red line). The black line shows the difference reflection spectrum from samples of groups 1 and 3 (in graphs 1 and 2, respectively).

results for noninvasive visualization in the dynamics of the development of pathology and monitoring the effectiveness of the treatment methods used.

As can be seen from Figs. 3–5, spectra are broadband and structureless. It shows the difference of groups on average, but it is impossible to select the optimal frequency for the analysis of differences. For an integrated assessment of the difference between the THz response of blood serum and water, we used the T_p value, which represents the peak amplitude of the THz pulse (Fig. 2), normalized to water transmission. Figure 6 shows the T_p value for each sample examined (Fig. 6a) and shows the dependence of this value on the protein content in the samples (Fig. 6b).

As can be seen from Fig. 6, the largest differences in the transmission spectrum are observed between rats of group 1 (healthy rats) and group 3 (28 days after tumor implantation), and these differences are associated with a decrease in the protein content in the blood serum of rats during tumor development.

In addition to the results of THz spectroscopy, the refractive index in the visible and near IR ranges (480–1550 nm) was measured for the same samples. Figure 7 shows the value of the refractive index at a wavelength of 589 nm from measured samples and the relationship between this refractive index and the serum protein content of the experimental groups. A similar relationship was obtained for other wavelengths.

The same tendencies are observed in the change in the optical characteristics of the serum of rats in the dynamics of tumor development and their dependence on the concentration of the most variable biochemical index: the protein content in the serum (Figs. 6, 7).

The Pearson correlation coefficients were calculated for a quantitative assessment of the coupling of optical parameters in the visible/IR and THz regions. The correlation coefficient between the values of

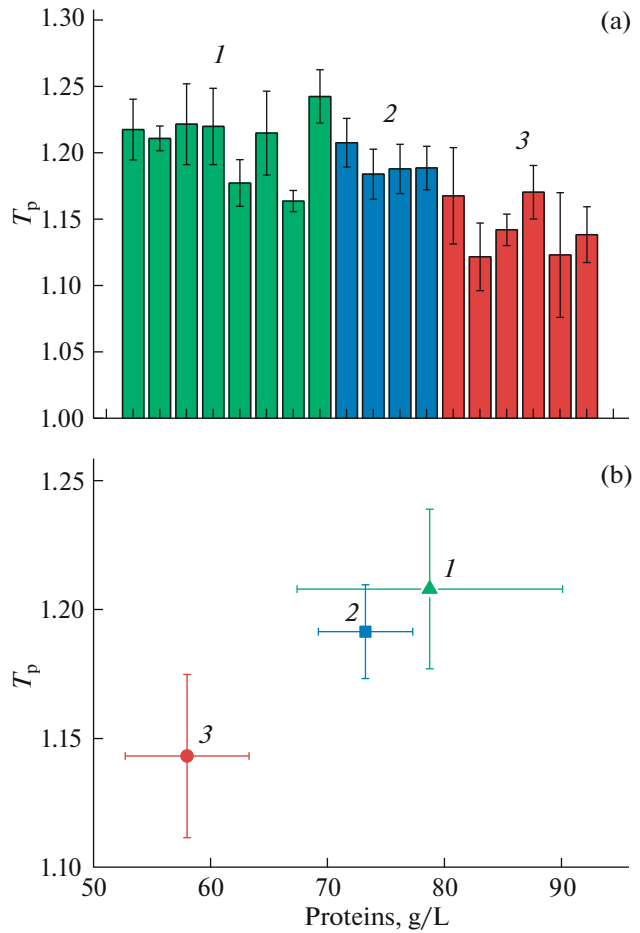


Fig. 6. (a) T_p values of the samples (the means from the triplicates); (b) the dependence of T_p values on the protein concentration in the samples. The means for each group are shown: (1) is group 1, (2) is group 2, (3) is group 3.

parameter T_p and the refractive index at a wavelength of 589 nm can be written as

$$\rho_{n_{589}, T_p} = \frac{\text{cov}(n_{589}, T_p)}{\sigma_{n_{589}} \sigma_{T_p}} = \frac{M\{[n_{589} - M(n_{589})][T_p - M(T_p)]\}}{\sigma_{n_{589}} \sigma_{T_p}}, \quad (11)$$

where $\sigma_{n_{589}}$ and σ_{T_p} are the standard deviations of the refractive index at a wavelength of 589 nm (n_{589}) and the normalized transmittance amplitude in the THz region (T_p) respectively; $M(n_{589})$ and $M(T_p)$ are the expected values of the variables; and $\text{cov}(n_{589}, T_p)$ is a covariation.

The average correlation coefficient calculated for each experimental group was 0.977 ± 0.034 , which indicates a high correlation of the data (Fig. 8).

The decrease in the refractive index in the visible region during the development of oncologic disease in

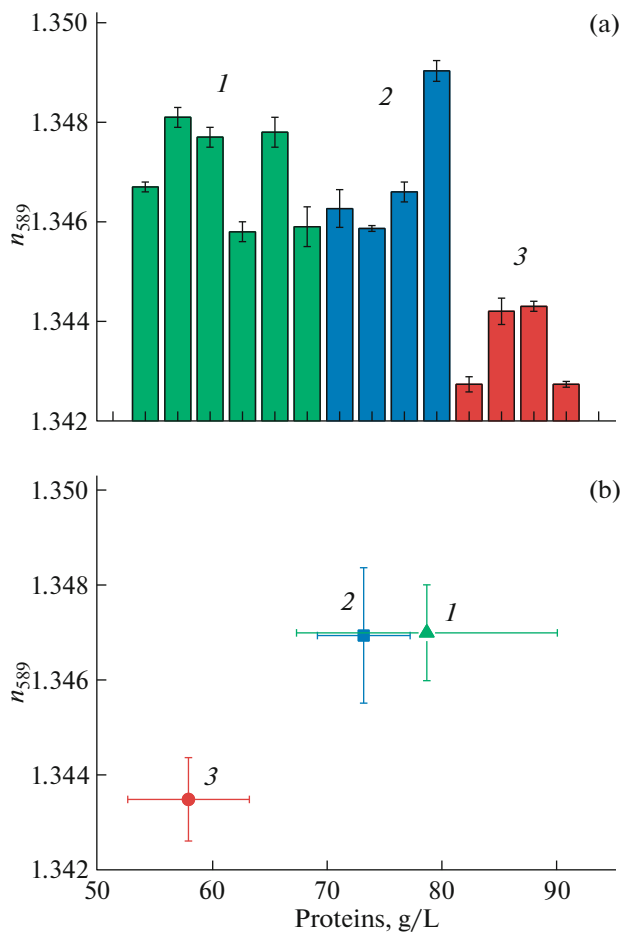


Fig. 7. (a) The value of the refractive index at a wavelength of 589 nm over samples (the mean of three measurements); (b) the relationship between the refractive index at a wavelength of 589 nm and the protein content in the serum of experimental groups. The means for each group are shown: (1) is group 1, (2) is group 2, (3) is group 3.

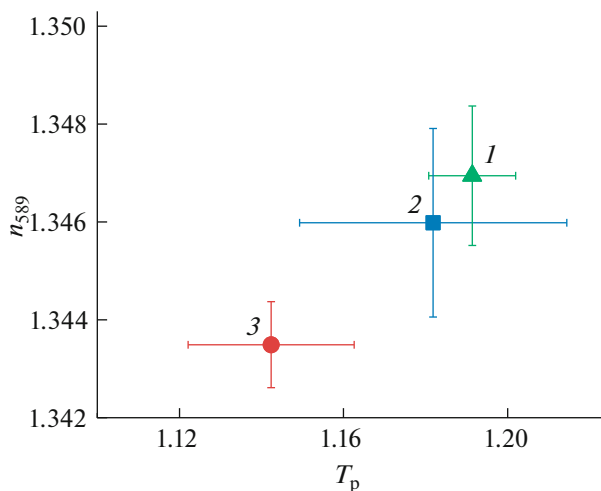


Fig. 8. The correlation between the refractive index at a wavelength of 589 nm and the normalized (to water) amplitude of the THz transmittance of T_p of the blood serum. The means for each group are shown: (1) is group 1 (triangles), (2) is group 2 (squares), (3) is group 3 (circles).

animals is due to a decrease in protein concentration, since the concentration of protein in the blood is linearly related to the refractive index [32]. The high correlation between the data in the THz and visible regions, for example, makes it possible to reconstruct the dispersion dependence in the THz region from known values of the refractive index in the visible region and from the absorption coefficient in the THz region using the Kramers–Kronig method [33].

CONCLUSIONS

We studied the transmission spectra in the frequency range of 0.05–1.0 of the samples of rat serum in the dynamics of experimental liver cancer. Serum samples of blood from healthy rats and individuals with grafted tumors were examined 14 and 28 days after the implantation of tumor cells. The development of this pathology is characterized by a statistically significant decrease in the concentration of both total protein and albumin in the blood. It was shown that the THz spectra of samples from healthy animals and from those with an implanted tumor have a similar shape, but differ in amplitude, which correlates with the protein content in samples determined biochemically.

Analysis of the observed differences was performed by comparing the experimental spectra obtained with a modified three-component relaxation model to describe the dielectric function of an aqueous solution. It was possible to analyze the characteristic differences for blood serum in normal conditions and in the pathology development. The observed changes in the THz response are due to the formation of bound water around the protein molecules; in samples of animals with cancer, the amount of protein and bound water is less. A model description of the dielectric function of samples from healthy and experimental animals (28 days after tumor implantation) predicts the maximum sensitivity of noninvasive THz diagnostics in the region of 100–300 GHz. The data on THz transmission spectra correlate well with the results of refractometric measurements in the visible and IR regions, which can be used as an additional method for constructing the dispersion dependence in the THz region. The potential advantage of THz diagnostics is the possibility of noninvasive and noncontact measurements, for example, using reflection spectroscopy from the skin, oral mucosa or conjunctiva of the eye.

FUNDING

This study was supported by the Russian Foundation for Basic Research (project no. 17-00-00275 (17-00-00270, 17-00-00272) in the medical–biological part and project no. 18-52-00040 in part of the development of THz technology.

COMPLIANCE WITH ETHICAL STANDARDS

All applicable international, national, and/or institutional guidelines for the care and use of animals have been implemented.

CONFLICT OF INTEREST

The authors declare no conflict of interest.

REFERENCES

- O. A. Smolyanskaya, N. V. Chernomyrdin, A. A. Konovko, K. I. Zaytsev, I. A. Ozheredov, O. P. Cherkasova, M. M. Nazarov, J. P. Guillet, S. A. Kozlov, Yu. V. Kistenev, J.-L. Coutaz, P. Mounaix, V. L. Vaks, J.-H. Son, H. Cheon, V. P. Wallace, et al., *Prog. Quantum Electron.* **62**, 1 (2018).
<https://doi.org/10.1016/j.pquantelec.2018.10.001>
- M. Nazarov, A. Shkurinov, V. V. Tuchin, and X.-C. Zhang, *Handbook of Photonics for Biomedical Science, Series in Medical Physics and Biomedical Engineering*, Ed. by V. V. Tuchin (CRC, Taylor and Francis, Boca Raton, 2010), p. 519.
- A. Charkhesht, C. K. Regmi, K. R. Mitchell-Koch, S. Cheng, and N. Q. Vinh, *J. Phys. Chem. B* **122**, 6341 (2018).
<https://doi.org/10.1021/acs.jpcc.8b02872>
- C. Reid, G. Reese, A. P. Gibson, and V. P. Wallace, *IEEE J. Biomed. Health Inform.* **17**, 774 (2013).
- A. J. Fitzgerald, E. Pickwell-MacPherson, and V. P. Wallace, *PLoS One* **9**, e99291 (2014).
- A. A. Angeluts, A. V. Balakin, M. G. Evdokimov, M. N. Esaulkov, M. M. Nazarov, I. A. Ozheredov, D. A. Sapozhnikov, P. M. Solyankin, O. P. Cherkasova, and A. P. Shkurinov, *Quantum Electron.* **44**, 614 (2014).
- S. Yamaguchi, Y. Fukushi, O. Kubota, T. Itsuji, T. Ouchi, and S. Yamamoto, *Sci. Rep.* **6**, 30124 (2016).
<https://doi.org/10.1038/srep30124>
- M. Borovkova, M. Khodzitsky, P. Demchenko, O. Cherkasova, A. Popov, and I. Meglinski, *Biomed. Opt. Express* **9**, 2266 (2018).
<https://doi.org/10.1364/BOE.9.002266>
- N. Chernomyrdin, A. Gavidush, S.-I. Beshplav, K. Malakhov, A. Kucheryavenko, G. Katyba, I. Dolganova, S. Goryaynov, V. Karasik, I. Spektor, V. Kurlov, S. Yurchenko, G. Komandin, A. Potapov, V. Tuchin, and K. Zaytsev, *Proc. SPIE* **10716**, 107160S (2018).
- Fundamental and Clinical Physiology*, Ed. by A. G. Kamkin and A. A. Kamenskii (Akademiya, Moscow, 2004) [in Russian].
- T.-F. Tseng, B. You, H.-C. Gao, T.-D. Wang, and C.-K. Sunet, *Opt. Express* **23**, 9440 (2015).
- S. I. Gusev, N. S. Balbekin, E. A. Sedykh, E. N. Grineva, and M. K. Khodzitsky, *J. Phys.: Conf. Ser.* **735**, 012088 (2016).
- K. Jeong, Y.-M. Huh, S.-H. Kim, Y. Park, J.-H. Son, S. J. Oh, and J.-S. Suh, *J. Biomed. Opt.* **18**, 107008 (2013).
- C. K. Sun, H. Y. Chen, T. F. Tseng, B. You, M.-L. Wei, J.-Y. Lu, Y.-L. Chang, W.-L. Tseng, and T.-D. Wang, *Sci. Rep.* **8**, 3948 (2018).
<https://doi.org/10.1038/s41598-018-22060-y>
- S. I. Gusev, P. S. Demchenko, O. P. Cherkasova, V. I. Fedorov, and M. K. Khodzitsky, *Chin. Opt.* **11**, 182 (2018).
- H. Chen, X. Chen, S. Ma, X. Wu, W. Yang, W. Zhang, and X. Liet, *J. Infrar. Millimeter Terahertz Waves* **39**, 399 (2018).
- O. P. Cherkasova, M. M. Nazarov, A. A. Angeluts, and A. P. Shkurinov, *Opt. Spectrosc.* **120**, 50 (2016).
- O. P. Cherkasova, M. M. Nazarov, I. N. Smirnova, A. A. Angeluts, and A. P. Shkurinov, *Phys. Wave Phenom.* **22**, 185 (2014).
- M. M. Nazarov, O. P. Cherkasova, and A. P. Shkurinov, *Quantum Electron.* **46**, 488 (2016).
- M. M. Nazarov, O. P. Cherkasova, and A. P. Shkurinov, *J. Phys.: Conf. Ser.* **793** (2017).
<https://doi.org/10.1088/1742-6596/793/1/012005>
- M. M. Nazarov, O. P. Cherkasova, and A. P. Shkurinov, *J. Infrar. Millimeter Terahertz Waves* **39**, 840 (2018).
- E. Shirshin, O. Cherkasova, T. Tikhonova, E. Berlovskaya, A. Priezzhev, and V. Fadeev, *J. Biomed. Opt.* **20**, 051033 (2015).
- O. A. Smolyanskaya, O. V. Kravtsenyuk, A. V. Panchenko, E. L. Odlyanitskii, Zh. P. Giie, O. P. Cherkasova, and M. K. Khodzitskii, *Quantum Electron.* **47**, 1031 (2017).
- Q.-X. Pan, Z.-J. Su, J.-H. Zhang, C.-R. Wang, and S.-Y. Ke, *Mol. Clin. Oncol.* **6**, 566 (2017).
- M. M. Nazarov, A. P. Shkurinov, A. A. Angeluts, and D. A. Sapozhnikov, *Izv. Vyssh. Uchebn. Zaved., Radiofiz.* **52**, 595 (2009).
- T. Fukasawa, T. Sato, J. Watanabe, Y. Hama, W. Kunz, and R. Buchner, *Phys. Rev. Lett.* **95**, 197802 (2005).
- M. M. Nazarov, A. P. Shkurinov, E. A. Kuleshov, and V. V. Tuchin, *Quantum Electron.* **38**, 647 (2008).
- M. Born and E. Wolf, *Principles of Optics: Electromagnetic Theory of Propagation, Interference and Diffraction of Light*, 7th ed. (Cambridge Univ. Press, Cambridge, 1999).
- A. B. Bucharskaya, N. I. Dikht, G. A. Afanas'eva, G. S. Terentyuk, N. B. Zakharova, G. N. Maslyakova, B. N. Khlebtsov, and N. G. Khlebtsov, *Saratov. Nauch.-Med. Zh.* **11**, 107 (2015).
- International Guiding Principles for Biomedical Research Involving Animals, CIOMS and ICLAS, 2012. <http://www.cioms.ch/index.php/12-news-flash/227-cioms-and-iclas-release-the-new-international-guiding-principles-for-biomedical-research-involving-animals>.
- O. P. Cherkasova, M. M. Nazarov, and A. P. Shkurinov, *Opt. Quant. Electron.* **48**, 217 (2016).
- A. N. Bashkatov, K. V. Berezin, K. N. Dvoretzkiy, M. L. Chernavina, E. A. Genina, V. D. Genin, V. I. Kochubey, E. N. Lazareva, A. B. Pravdin, M. E. Shvachkina, P. A. Timoshina, D. K. Tuchina, D. D. Yakovlev, D. A. Yakovlev, I. Yu. Yanina, et al., *J. Biomed. Opt.* **23**, 091416 (2018).
- O. Sydoruk, O. Zhernovaya, V. Tuchin, and A. Douplik, *J. Biomed. Opt.* **17**, 115002 (2012).

Translated by I. Shipounova